Redox Biology 21 (2019) 101071

Contents lists available at ScienceDirect

Redox Biology

journal homepage: www.elsevier.com/locate/redox

Research Paper

# Red fluorescent redox-sensitive biosensor Grx1-roCherry

Arina G. Shokhina[a], Alexander I. Kostyuk[a], Yulia G. Ermakova[a,b], Anastasiya S. Panova[a], Dmitry B. Staroverov[a], Evgeny S. Egorov[a], Mikhail S. Baranov[a], Gijsbert J. van Belle[c], Dörthe M. Katschinski[c], Vsevolod V. Belousov[a,c,d,*], Dmitry S. Bilan[a,d,*]

[a] Shemyakin-Ovchinnikov Institute of Bioorganic Chemistry, Moscow 117997, Russia
[b] European Molecular Biology Laboratory, Heidelberg 69117, Germany
[c] Institute for Cardiovascular Physiology, Georg August University Göttingen, Göttingen 37073, Germany
[d] Pirogov Russian National Research Medical University, Moscow 117997, Russia

ARTICLE INFO

*Keywords:*
Grx1-roCherry
2GSH/GSSG
Redox-sensitive fluorescent protein
Biosensor
Multiparameter imaging

ABSTRACT

Redox-sensitive fluorescent proteins (roFPs) are a powerful tool for imaging intracellular redox changes. The structure of these proteins contains a pair of cysteines capable of forming a disulfide upon oxidation that affects the protein conformation and spectral characteristics. To date, a palette of such biosensors covers the spectral range from blue to red. However, most of the roFPs suffer from either poor brightness or high pH-dependency, or both. Moreover, there is no roRFP with the redox potential close to that of 2GSH/GSSG redox pair. In the present work, we describe Grx1-roCherry, the first red roFP with canonical FP topology and fluorescent excitation/emission spectra of typical RFP. Grx1-roCherry, with a midpoint redox potential of − 311 mV, is characterized by high brightness and increased pH stability (pKa 6.7). We successfully used Grx1-roCherry in combination with other biosensors in a multiparameter imaging mode to demonstrate redox changes in cells under various metabolic perturbations, including hypoxia/reoxygenation. In particular, using simultaneous expression of Grx1-roCherry and its green analog in various compartments of living cells, we demonstrated that local $H_2O_2$ production leads to compartment-specific and cell-type-specific changes in the 2GSH/GSSG ratio. Finally, we demonstrate the utility of Grx1-roCherry for *in vivo* redox imaging.

## 1. Introduction

Glutathione is a tripeptide that is widespread in the cells of most organisms. The thiol group of the cysteine residue in the second position plays a key role in glutathione function. In a cell, glutathione can exist in reduced (GSH) and oxidized forms (GSSG). The molecule of GSH is able to donate a reducing equivalent to acceptor molecules. This reaction can be associated with the reduction of lipid peroxides and hydrogen peroxide protecting cells from the oxidative stress caused by the generation of reactive oxygen species (ROS). Since the ROS are formed in the cell spontaneously but also purposefully for the regulation of certain biological processes, the glutathione peroxidase reaction, as well as other thiol peroxidases, is essential for turning off redox signals. Some disulfide bonds (-S-S-) in proteins are formed and reduced by representatives of the glutaredoxin protein family (Grx), equilibrating protein thiols with a 2GSH/GSSG redox state [1–3]. Glutathione disulfide can be reduced to GSH *via* a reaction catalyzed by glutathione reductase using NADPH and FAD as cofactors [3]. The ratio of the reduced form of glutathione to the oxidized form (the 2GSH/GSSG ratio) is maintained by a cellular system within a certain range, which depends on the cell type and compartment. In summary, the 2GSH/GSSG ratio is an important biological parameter that determines the overall cellular redox status.

A study of the redox state of the cellular glutathione pool is necessary both for understanding the mechanisms of physiological processes and for pathological processes caused by disturbances of the

*Abbreviations:* 2-AAPA, 2-acetylamino-3-[4-(2-acetylamino-2-carboxyethylsulfanylthiocarbonylamino)phenylthiocarbamoylsulfanyl]propionic acid; cpFP, circularly permuted fluorescent protein; cpmApple, circularly permuted monomeric Apple; cpYFP, circularly permuted yellow fluorescent protein; DAO, D-amino-acid oxidase; DAO-mito, DAO localized in the mitochondrial matrix; DAO-NLS, DAO localized in the nucleus; DCA, dichloroacetate; DMF, dimethyl fumarate; FP, fluorescent protein; Grx, glutaredoxin; NRF2, nuclear factor (erythroid-derived 2)-like 2; roFP, redox-sensitive fluorescent protein; roGFP, redox-sensitive green fluorescent protein; ROS, reactive oxygen species; rxRFP, redox-sensitive red fluorescent protein; rxYFP, redox-sensitive yellow fluorescent protein; Trx, thioredoxin; TrxR, thioredoxin reductases

* Corresponding authors at: Shemyakin-Ovchinnikov Institute of Bioorganic Chemistry, Moscow 117997, Russia.
*E-mail addresses:* belousov@ibch.ru (V.V. Belousov), d.s.bilan@gmail.com (D.S. Bilan).

https://doi.org/10.1016/j.redox.2018.101071
Received 10 October 2018; Received in revised form 5 December 2018; Accepted 6 December 2018
Available online 07 December 2018

thiol-disulfide exchange. Some synthetic dyes, for example, Ellman's reagent [4], ThiolQuant Green [5], and RealThiol [6] can be used to quantify changes in GSH level. However, a breakthrough in studies in the field of redox biology has occurred with the advent of genetically encoded biosensors based on fluorescent proteins [7]. Such biosensors are a powerful tool for exploring biological processes in living systems in real time. Since the molecule is encoded by a gene, the biosensor can be directed to any tissues of the researched organism or particular cell organelles. With the development of such tools, it became possible to monitor the dynamics of hydrogen peroxide ($H_2O_2$) [8–12], the redox state of NAD(H) [13–16] and NADP(H) [17,18] pools in the complex living systems. Several biosensors have been developed to date to visualize the dynamics of the change in the 2GSH/GSSG ratio. The principle of function of these biosensors is based on a pair of surface-exposed cysteine residues introduced into the structure of a fluorescent protein into adjacent β-sheets. Cysteine residues form a disulfide bond during oxidation, leading to conformational shifts in the structure, which is reflected in changes in the protein spectral characteristics. When the disulfide bond of the protein is reduced, the fluorescent signal returns to its initial value. Since the cellular thiol groups are in redox equilibrium with the glutathione pool, roFPs can be used to monitor changes in the 2GSH/GSSG ratio. The first biosensor of this family, called rxYFP, was developed based on a yellow fluorescent protein (YFP) [19]. Then, redox active versions of roGFP1 and roGFP2 were developed on the basis of a green fluorescent protein (GFP). These versions have several advantages. In particular, both demonstrate a ratiometric signal that is not sensitive to pH changes in the physiological range [20,21]. To date, there is an extensive collection of roGFP versions that differ in various parameters, including the midpoint redox potential and reaction rate [22]. Alone, rxYFP and roGFP slowly equilibrate with redox state of the glutathione pool. However, if the local level of Grx is increased, the reaction proceeds much faster. For example, the dynamic characteristics of rxYFP and roGFP2 were significantly improved after these proteins were fused with Grx *via* a polypeptide linker [23,24].

At present, biosensors for monitoring the redox status of the glutathione pool, based on redox-active FP, are very popular and are used in various studies, including *in vivo* studies [22]. Most of the existing biosensors, not only roFPs, have similar spectral characteristics, since they were developed on the basis of green-emitting proteins. This fact imposes a significant limitation on the use of these tools in the multiparameter imaging mode in combination with other spectrally distinct fluorophores. This approach allows the simultaneous monitoring of either different activities within the same cellular organelle or the same parameter in different organelles of the cell or even in different types of cells within the tissue [25]. As a result, new spectral versions of roFPs are being developed. For example, biosensors for the 2GSH/GSSG ratio have been developed based on blue fluorescent proteins [26]. It must be recognized that proteins with blueshifted spectra have some limitations when working with living objects, especially *in vivo*. Excitation light with a shorter wavelength is more toxic for cells. In addition, for such imaging parameters (excitation by violet light), biological objects are characterized by a high level of autofluorescence. Red proteins do not have such drawbacks.

A biosensor for monitoring the redox state of the glutathione pool based on red fluorescent protein, rxRFP, has also been developed [27]. It differs in design from all other roFPs. The basis of rxRFP is the circularly permuted red fluorescent protein cpmApple. The circularly permuted FP (cpFP) differs from its original variant in the presence of the N- and C-termini near the chromophore, while the native termini are ligated by a polypeptide linker. The structure of this protein becomes more labile and susceptible to conformational changes. The cpYFPs are used in many existing biosensors. For example, cpmApple is part of the biosensors used to image calcium (R-GECO1) [28] and $H_2O_2$ (HyPerRed) [11]. In rxRFP, redox-active cysteines are located at the N- and C- termini of cpFP, unlike other biosensors in which the mutations were introduced directly into the structure of the nonpermutated β-barrel. The reversible formation of a disulfide bond between the N- and C- termini leads to changes in the spectral characteristics of rxRFP [27]. rxRFP is not fused with Grx. Thus, its redox state is equilibrated by the endogenous cellular Grx pool.

Another redox FP with red emission, roRFP [29] has large Stokes shift and its excitation is 420 nm that is extremely short wavelength for RFP. However, due to combination of extremely low redox potential, pH sensitivity and unusual spectral properties this mKeima based roFP did not find its users yet.

In this paper, we present a new biosensor for the 2GSH/GSSG ratio based on RFP mCherry [30]. To produce the biosensor Grx1-roCherry, we introduced two cysteine residues into the structure of the native barrel of mCherry, placing them on adjacent β-sheets. To increase the dynamic characteristics, roCherry was fused to the human Grx1 *via* a polypeptide linker. In this work, we have demonstrated that Grx1-roCherry can be successfully used in combination with other redox biosensors in a multiparameter imaging mode.

## 2. Materials and methods

### 2.1. Construct design and cloning

Grx1-roCherry was developed by fusion of human Grx1 and FP mCherry DNA sequences *via* a synthetic linker consisting of 15 amino acid residues (SGTGGNASDGGGSGG) (linker from Peredox biosensor [31]). Grx1 and mCherry were amplified from previously described vectors pQE-60 Grx1-roGFP2-His (Addgene # 64799) [24] and pcDNA-PhoCl-mCherry-myc (Addgene # 87692) [32]. Primers for Grx1: 5′-ATCGATGCCACCATGGCTCAAGAGTTTGTGAACTGCAAAA-3′ and 5′-CTAAAGCAGATTGGAGCTCTGCAGACTTCCGGAACTGGGGGCAACG CCTCTGACGGTGGT-3′; primers for mCherry: 5′- CAACGCCTCTGACG GTGGTGGGTCTGGTGGTGTGAGCAAGGGCGAGGAGGATAA-3′ and 5′-TCTAGATTAAGTCTGCAGAGCTCCAATCTGCTTTAGC-3′. Fragments obtained using these primers were combined into a whole construct of Grx1-mCherry by “overlap extension” PCR. The construct was cloned into a pCS2+ vector (Xenbase) using restriction sites *ClaI/Xba*I. We inserted a pair of redox-sensitive cysteines, Ala150Cys/Lys203Cys, with additional Thr after Cys150 and substitution Ser151Glu by site specific mutagenesis, using the following primers: 5′-GGGCTGGGAGtgcTCCT CCG-3′ and 5′-CGGAGGAGCACTCCCAGCCC-3′ (for Ala150Cys), 5′-AACGTCAACATCtgcTTGGACATCACCTCC-3′ and 5′-GGAGGTGATG TCCAAGCAGATGTTGACGTT-3′ (for Lys203Cys), 5′-GGGAGTGCACCT CCTCCGA-3′ and 5′-TCGGAGGAGGTGCACTCCC-3′ (for insertion of Thr after Cys150), 5′-GGAGTGCACCGAATCCGAGC-3′ and 5′-GCTCGGATT CGGTGCACTCC-3′ (for Ser151Glu). We also generated a version of the biosensor without Grx1 using the primers 5′-ATCGATGCCACCATGGT GAGCAAGGGCGAGGA-3′, 5′-TCTAGATTAAGTCTGCAGAGCTCCAATC TGCTTTAGC-3′ and constructed pCS2 + Grx1-roCherry as a template. For bacterial expression, we have used Grx1-roCherry with 6 × His tag on the C-terminus, which was cloned into the pQE30 plasmid (Qiagen) using the restriction sites BamHI/HindIII.

### 2.2. Protein expression and purification

To purify the Grx1-roCherry biosensor, *E. coli* XL1Blue cells were transformed with pQE30-Grx1-roCherry plasmid. Bacteria were grown on LB-agar plates with ampicillin (100 μg/ml) for 14 h at 37 °C. Plates with bacterial colonies were incubated for 24 h at 17 °C for the folding and chromophore maturation of Grx1-roCherry. In the next step, colonies were washed from the agar surface with PBS buffer (137 mM NaCl, 2.7 mM KCl, 10 mM $Na_2HPO_4$, 1.8 mM $KH_2PO_4$, pH = 7.4) containing 5 mM 2-mercaptoethanol. The total volume of the suspension was adjusted to 30 ml using the same buffer, and the sample was sonicated in an ice bath for 30 min (Sonic Vibra cell) using the following program: 5 s sound:10 s pause cycle with amplitude of 32%. Thereafter,

cell lysates were centrifuged at 20,000 × *g*, 4 °C for 25 min. Proteins were purified from the supernatant using metal affinity chromatography (Talon Metal Affinity Resin, Clontech). Total samples were applied to a column filled with 3.5 ml of resin that was previously equilibrated with PBS, containing 5 mM 2-mercaptoethanol. To eliminate nontarget soluble compounds, the column was washed with 25 ml of the same buffer and the protein was eluted with PBS containing 250 mM imidazole and 5 mM 2-mercaptoethanol. To remove imidazole and reducing agent purified Grx1-roCherry was applied to a 10 ml Sephadex G-25 column (GE Healthcare) equilibrated with PBS. All buffers were kept on an ice bath throughout the entire procedure. Grx1-roGFP2 was purified according to the same protocol.

To obtain a fully reduced form of the probe, the samples were incubated on an ice bath in the presence of 20 mM DTT for one hour. The DTT was removed by centrifugation using Amicon Ultra-0.5 ml Centrifugal Filters at 14.000 × *g*, 4 °C for 35 min.

### 2.3. In vitro characterization of Grx1-roCherry

Since Grx1-roCherry is difficult to purify in a fully reduced form, the spectroscopic properties of the biosensor were determined only for the oxidized form. To establish the absorption maximum of the probe, an aliquot of Grx1-roCherry purified protein was diluted in 1 ml of PBS, and its absorption spectra was recorded in the range of 400–700 nm. The molar extinction coefficient was determined using the equation $\varepsilon = A*C(M)^{-1} *L(cm)^{-1}$, where A is the optical density at the absorption maximum, C is the protein concentration and L is the optical path length. To determine the quantum yield (QY) of fluorescence of Grx1-roCherry, the emission spectrum excited at 589 nm was measured and compared with corresponding data for the mCherry protein at the same molar concentration. All calculations were performed according to the formula $QY_{Grx1\text{-}roCherry} = QY_{mCherry}* (A_{mCherry}*Em_{Grx1\text{-}roCherry} *A_{Grx1\text{-}roCherry}{}^{-1} *Em_{mCherry}{}^{-1})$ where A is the optical density at the absorption maximum and Em is the emission intensity at emission maximum; $QY_{mCherry}$ is a standard value (0.22). The absorption maxima for mCherry and Grx1-roCherry were 589 nm. The emission maxima for mCherry and Grx1-roCherry were 610 nm. The molar concentrations of proteins were determined using a Bicinchoninic Acid Protein Assay Kit (Sigma). The intensities of Grx1-roCherry and mCherry fluorescence were recorded using a Varian Cary Eclipse spectrophotometer.

To determine the apparent pKa of Grx1-roCherry a set of standard buffers with known pH values (3.0–9.5) was prepared. The buffers had the following compositions: pH = 3.0 (40 mM $Na_3C_6H_5O_7$–60 mM HCl), pH = 3.5 (47 mM $Na_3C_6H_5O_7$–53 mM HCl), pH = 4.0 (56 mM $Na_3C_6H_5O_7$–44 mM HCl), pH = 4.5 (80 mM $Na_3C_6H_5O_7$ –28 мМ mM), pH = 5.0 (0.63 mM $Na_2HPO_4$–65 mM $KH_2PO_4$), pH = 5.5 (2.6 mM $Na_2HPO_4$–63 mM $KH_2PO_4$), pH = 6.0 (7 mM $Na_2HPO_4$–60 mM $KH_2PO_4$), pH = 6.5 (20 mM $Na_2HPO_4$–45 mM $KH_2PO_4$), pH = 7.0 (40 mM $Na_2HPO_4$–25 mM $KH_2PO_4$), pH = 7.5 (56 mM $Na_2HPO_4$–9.8 mM $KH_2PO_4$), pH = 8.0 (28 mM $Na_2B_4O_7$–44 mM HCl), pH = 8.5 (31 mM $Na_2B_4O_7$–38 mM HCl), pH = 9.0 (43 mM $Na_2B_4O_7$–14 mM HCl), and pH = 9.5 (39.5 mM $Na_2B_4O_7$–21 mM NaOH). The pH-titration of the probe was performed *via* the addition of concentrated aliquots (5 µl, in PBS) of the reduced biosensor into 1 ml of the above-described buffers. The intensity of Grx1-roCherry emission in each of the buffers was recorded using a Varian Cary Eclipse spectrophotometer.

Grx1-roCherry is highly sensitive to GSSG. To determine Grx1-roCherry's ability to sense reduced GSH, an aliquot of the oxidized biosensor was diluted in PBS containing 1 mM GSH, 2 mM NADPH and 0.5–1.5 U/ml glutathione reductase from baker's yeast (Sigma). The final concentration of the biosensor in the sample was 40 nM. The probe was incubated for 40 min at room temperature, and we measured emission intensity using a Varian Cary Eclipse spectrophotometer. NADPH and glutathione reductase are required to eliminate the traces of oxidized glutathione that are present in commercially available GSH reagent.

In another set of experiments, we tested the selectivity of Grx1-roCherry. Various oxidants were added to biosensor samples (40 nM) in PBS. In all tests, changes in emission intensity were registered immediately after mixing and during the next 10 min. In parallel control probes, aliquots of oxidant were substituted with PBS in the same volumes. To produce the superoxide anion radical in the probe, we used 50 µM xanthine and 0.25 U/ml xanthine oxidase (Sigma). NO was generated in the probe using MAHMA NONOate (Sigma).

Experiments to determine the midpoint redox potential were performed in PBS, pH = 7.4. As a redox couple, we used $DTT_{reduced}$ and $DTT_{oxidized}$. The total concentration of DTT in both forms was 1 mM, protein concentration was 40 nM, same as in other *in vitro* tests. The incubation time was 3 h at room temperature. Grx1-roGFP2 was used as a control with a known potential value. The signals were calculated as emission intensity at 610 nm and 395 nm/489 nm excitation ratio for Grx1-roCherry and Grx1-roGFP2, respectively. The obtained values were normalized to the smallest ones and plotted against redox potentials of corresponding buffers.

### 2.4. Cell cultures

We cultured HeLa Kyoto and HEK293 (ATCC) cells in RPMI1640 (PanEko) supplemented with 10% FBS (Biosera), 2 mM L-glutamine (PanEko), 100 U/ml penicillin (PanEko) and 100 mg/ml streptomycin (PanEko) at 37 °C in a 5% $CO_2$ atmosphere. For imaging experiments, cells were seeded into 35 mm glass bottom FluoroDishes (World Precision Instruments). After 24 h, cells were transfected with plasmids for the required biosensor using FuGeneHD transfection reagent (Promega) according to the manufacturer's recommendations.

The mixed mouse primary embryonic cortex neuronal cell culture was prepared according the protocol for animal handling approved by the ethical committee of the Institute of Bioorganic Chemistry of the Russian Academy of Science. Embryos of C57Bl/6 mice at E17 were extracted and anesthetized in cold HBSS with low $Mg^{2+}$ and $Ca^{2+}$. Brains were extracted and piled from meninges. Cortices were collected in cold HBSS during the extraction process and then transferred to a 0.05% solution of trypsin/EDTA (PanEko) for 15 min at 37 °C and washed three times with warm Neurobasal medium (Gibco), which contained B27 (Gibco), 10% heat-inactivated FBS and 2 mM GlutaMax (Gibco). The cortices were gently triturated; neurobasal medium was added to obtain 1.5 million cells per 1 ml of medium. This cell suspension was seeded into the preliminary covered with poly-D-lysine (Invitrogen) 35 mm FluoroDishes (World Precision Instruments) (100 µl per dish). At 1 h, plated cells were covered with 2 ml of neurobasal medium, and then 1/3 of its volume was exchanged with fresh medium every three days. Five days later, the mixed mouse primary embryonic cortex neuronal cell culture was transfected with Lipofectamine LTX (Invitrogen) according to the manufacturer's recommendations.

### 2.5. Fluorescence microscopy for imaging of living cells

For most experiments, cell imaging was performed using a Leica DMI6000, equipped with an HCX PL Apo CS 40.0 × 1.25 Oil UV objective, HCX PL APO lbd. BL 63 × 1.4NA oil objective, TX2 and GFP filter cubes, at 37 °C in Tyrode solution (Sigma) with 20 mM HEPES (PanEko) and 20 mM D-glucose. For titration of Grx1-roGFP2 and Grx1-roCherry in the same cells, we used µ-slides (IBIDI) and a confocal fluorescence microscope (Olympus FV1200). For Grx1-roGFP2, we used 405 nm (4%, 730 HV) and 488 nm (1.9%, 630 HV) laser lines; for Grx1-roCherry – 559 nm (3.9%, 730 HV). To determine the response of the probes to $H_2O_2$, we added a solution of $H_2O_2$ to a final concentration of 10–300 µM. The final processing of images was performed using ImageJ software.

For experiments with DMF treatment, we incubated cells in the medium with 50 µM DMF (Sigma) for 24 h. We used DMSO as the

negative control. To induce intracellular $H_2O_2$-generation by DAO, we used D-norvaline (Sigma). We added the solution of D-norvaline to cells at 100 µl volume obtain a final concentration of 2 mM. For experiments with TrxR inhibition, we incubated the cells in medium with 2.5 µM auranofin (Enzo) overnight, using DMSO as the negative control.

### 2.6. Flow cytometry

For experiments with DCA (Sigma), we incubated cells in medium with 30 mM DCA for 48 h, and cells were detached with 0.25% solution of trypsin (PanEko) and transferred to PBS (Santa Cruz Biotechnology) with 1% of FBS (PanEko). We detected the signals of the biosensors Grx1-roCherry, SoNar and SypHer2 using FACS Aria III (BD Biosciences, Franklin Lakes, NJ, USA). The obtained data were exported with Cytobank (https://www.cytobank.org/) to csv-format and were processed in RStudio.

### 2.7. Model of hypoxia

For hypoxia experiments, we incubated HeLa Kyoto cells in RPMI1640 medium containing no serum and no phenol red, but with sodium bicarbonate (2 g/L) for 1 h before imaging. The imaging was performed in 500 µl of the same medium with the inverted Olympus IX83 widefield microscope, equipped with a 60 × UPLS Apo/1.35 objective. Experiments were performed with the cellVivo incubation setup (Pecon) in normoxic conditions at 37 °C, 5% $CO_2$, 21% $O_2$ or in hypoxic conditions at 37 °C, 5% $CO_2$, 0% $O_2$.

### 2.8. Zebrafish husbandry and in vivo imaging

*D. rerio* (AB/TL strain) was handled according the protocol approved by the ethical committee of the Institute of Bioorganic Chemistry RAS. Embryos were raised in E3 medium (5 mM NaCl, 0.17 mM KCl, 0.33 mM CaCl2, 0.33 mM MgSO4, equilibrated to pH 7.0), which was also used as the imaging medium. We obtained larvae that transiently expressed Grx1-roCherry *via* microinjection of the mRNA into a yolk sac of 1-cell stage embryos. For *in vitro* mRNA synthesis, we used an mMessage mMachine SP6 Transcription kit (Ambion). Prepared mRNA was injected into the embryos' yolk at a 1 nl volume to a final concentration of 100 ng/µl. Injected larvae were kept in Petri dishes in the facility with a 12:12 light and night cycle at 28 °C. Then, 48 h after fertilization, embryos were screened with a Leica DMI6000 widefield microscope equipped with an HC PL FLUOTAR 10.0 * 0.30 DRY objective and TX2 BP560/40 filter cube. All animals subjected to experimentation were anesthetized in 0.02% MS-222, tricaine (Sigma). Before microscopy, embryos were manually extracted from chorions and embedded in 2% agarose in 35 mm glass-bottom FluoroDishes. To detect the response to oxidation of Grx1-roCherry expressed in zebrafish tissues, we added $H_2O_2$ (100 µl) to the embedded embryo to a final concentration of 50 mM.

## 3. Results

### 3.1. Engineering and screening of redox-sensitive red fluorescent protein

We selected mRuby2 [33] and mCherry [30] as candidate RFPs for the development of a redox-sensitive red fluorescent protein. We created several genetic constructs on the basis of these proteins, which differed in the arrangement of cysteine residues, and which we introduced using site-directed mutagenesis. We chose mutation positions satisfying two criteria: first, the cysteine residues were introduced in close proximity to the chromophore and, second, were placed close to each other to allow the formation of a disulfide bridge. Pairs of cysteine residues were introduced at positions 146–166, 146–203, 147–166, 147–203 of mRuby2 and 149–169, 149–203, 150–169, 150–203 of mCherry. By analogy with Grx1-roGFP2 [24], all our tested versions were fused at the N-termini to the human Grx1 *via* a polyglycine $(GGSGG)_6$ linker.

All versions were expressed in *E. coli*. All variants of red proteins were fluorescent. To determine the functional activity of the resulting variants of the biosensor, we added high concentrations of $H_2O_2$ (5 mM) to the bacterial suspensions. $H_2O_2$ is a powerful oxidizing agent, which in excess oxidizes the intracellular glutathione pool. As a result, only three versions, Grx1-mRuby2-E146C/R203C, Grx1-mCherry-A150C/R169C and Grx1-mCherry-A150C/K203C reacted to the oxidant with a change in the fluorescence emission spectrum. However, the amplitude of the response was not more then 10–15% for all constructs. Similar results were obtained after testing the same versions in eukaryotic cells. In HeLa Kyoto cells, Grx1-mCherry-A150C/K203C demonstrated an increase in fluorescence intensity by 16% after the addition of 2 mM of $H_2O_2$. The signal of the Grx1-mRuby2-E146C/R203C version under the same conditions decreased by 13%. Grx1-mCherry-A150C/R169C in these cells did not react to oxidation. We chose Grx1-mCherry-A150C/K203C for further improvement because this version was also visually distinguished from the others by high brightness.

Next, we tried to optimize the selected version. First, we replaced the $(GGSGG)_6$ linker between Grx1 and mCherry-A150C/K203C with a SGTGGNASDGGGSGG linker. Previously, this linker was used in the Peredox biosensor for the $NAD^+$/NADH ratio [13]. The brightness of this version was much higher than the parent variant. However, the signal amplitude in HeLa Kyoto cells remained the same. Therefore, linker composition can be essential for the spectral properties of roFPs.

Next, we rationalized that the poor amplitude of the probe's response could result from the low conformational flexibility of the chromophore environment. To enhance the mobility of the protein structure upon disulfide formation, we decided to introduce an additional amino acid residue into the protein sequence of mCherry-A150C/K203C at the position after redox-active Cys150. We tested the versions with insertions of all proteinogenic amino acids (except cysteine) in eukaryotic cells. As a result, we selected a version with an additional Thr residue after Cys150, the maximum response of which after oxidation was approximately 33%, which is 2-fold higher than in the original version. We then assumed that the introduction of polar amino acid residues into the chromophore environment of the biosensor can also affect its spectral characteristics, including increased dynamic range. For this purpose, we replaced the Ser151 residue with Thr, Asn, Gln, Asp and Glu, and replaced Glu153 with Thr, Asn, Gln and Asp. Among all these variants, only the Ser151Glu mutation turned out to be key. The fluorescence intensity of this version increased in cells approximately 2-fold during the maximal oxidation caused by the addition of $H_2O_2$.

Our final construct, containing Ala150Cys, Ser151Glu and Lys203Cys mutations and an additional insertion of Thr after the Cys150 residue, was called Grx1-roCherry. The structure of the protein is presented in the scheme (Fig. 1A). The minimal concentration of $H_2O_2$, which is necessary for the complete oxidation of the biosensor in the cells, is 150 µM. The biosensor reaches its maximum oxidation state in about 40 s. In addition, this version also demonstrates fast reversible reduction (Fig. 1B,C). Before detailed characterization of Grx1-roCherry, we confirmed that Grx1 play a key role in functioning of the biosensor. The version without Grx1 did not respond to $H_2O_2$ in the cells (Fig. 1B). In addition, we found that the roCherry construction with Grx1 at the C-terminus demonstrates the same response signal as Grx1-roCherry.

### 3.2. In vitro characterization of Grx1-roCherry

To study the properties of Grx1-roCherry, we extracted and purified the biosensor from *E. coli* XL1Blue using metal affinity chromatography. All buffers for protein extraction contained 5 mM 2-mercaptoethanol (2-ME) to avoid oxidation of the redox-sensitive cysteine residues. Purified Grx1-roCherry is characterized by a single excitation and a

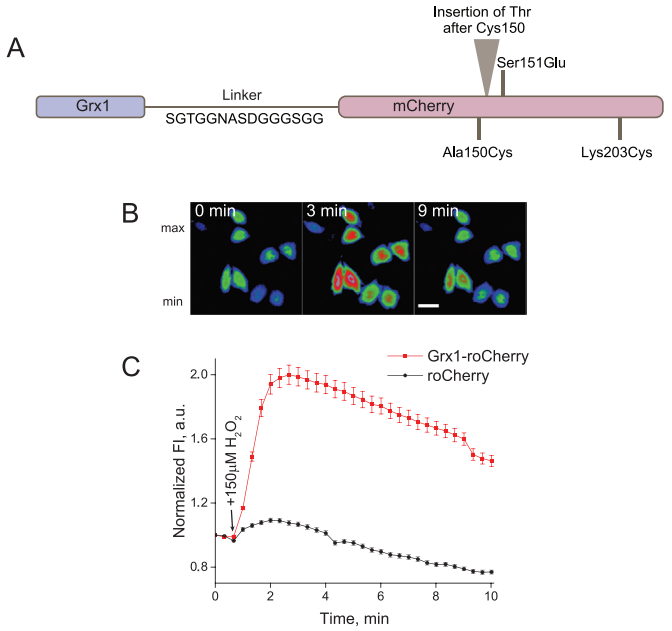


**Fig. 1.** Redox-sensitive biosensor Grx1-roCherry. (A) Diagram of Grx1-roCherry structure. Grx1-roCherry consists of a mutated fluorescent protein mCherry, a human glutaredoxin 1 and a polypeptide linker. The diagram shows the pair of redox-active cysteine residues and other mutations in the biosensor structure. (B) Images of Grx1-roCherry in transiently transfected HeLa Kyoto cells exposed to 150 μM of $H_2O_2$ after 40 s of imaging. Numbers indicate timing in seconds. Scale bar, 40 μm. Lookup table indicates intensity of red fluorescence. (C) Timing of $H_2O_2$ induced fluorescence change ($F_{589}$) in HeLa Kyoto cells expressing Grx1-roCherry (red line) or roCherry without Grx1 (black line). Signal values of Grx1-roCherry and roCherry were normalized to the initial value. Signals were averaged from 67 cells for Grx1-roCherry and 101 cells for roCherry in 3 experiments. Error bars indicate standard error of mean. (For interpretation of the references to color in this figure legend, the reader is referred to the web version of this article).

single emission maximum located at 589 and 610 nm, respectively (Fig. 2A). Incubation of the biosensor in the presence of 1 mM GSSG or 1 mM GSH (with addition of 2 mM NADPH and 0.5–1.5 U/ml glutathione reductase for elimination of GSSG traces) revealed that the intensity of fluorescence increases with oxidation (Fig. 2B). The same effect can be reproduced by incubation of the protein in the presence of millimolar concentrations DTT or 2-ME.

Purified Grx1-roCherry demonstrates fast response to different concentrations of GSSG (from 3 μM to 1 mM). $H_2O_2$ does not cause changes in the fluorescent signal of this probe (Fig. 2C).

Brightness estimation was performed by comparing the optical properties of Grx1-roCherry with the control protein mCherry. The molar extinction coefficient for oxidized Grx1-roRFP was ~ 14,500 $M^{-1}$ $cm^{-1}$. The value for mCherry was ~ 72,000 $M^{-1}$ $cm^{-1}$, indicating that molecular rearrangements implemented for the biosensor design significantly affected this parameter. Next, we measured a quantum yield of fluorescence that amounted to ~ 0.23, which was not significantly different from mCherry (~ 0.22). Finally, the brightness was calculated as product of the extinction coefficient and quantum yield. The estimated value was ~ 3335, which means that intact mCherry protein is approximately 4.75-fold brighter.

The acid-base properties of Grx1-roCherry were studied by the addition of protein aliquots to a row of standard buffers with known pH. The fluorescence increased 87-fold from pH 3.0–9.5, with an apparent pKa of 6.7 (Fig. 2D). In the physiological range (6.0–8.0) the change in emission intensity was ~ 4-fold. This is approximately 5.5 fold less than the much more pH-sensitive roRFP, based on cpmApple.

To test Grx1-roCherry selectivity, we prepared a reduced form of the biosensor by incubating purified protein in the presence of 20 mM DTT on an ice bath. Grx1-roGFP2 was taken as a control and was subjected to the same treatment. After the elimination of DTT, aliquots of reduced biosensors were diluted in PBS, with subsequent oxidant addition (Fig. 2E). The maximal amplitude of the Grx1-roCherry response to a saturating GSSG concentration of 1 mM was 1.53 ± 0.03 (mean ± s.e.m., here and after). Much smaller concentrations (10 μM) of GSSG still led to full oxidation of the probe, with an amplitude of 1.52 ± 0.03. In both cases, the spectrum of the sensor stabilized within several seconds after the addition, indicating that interactions between the sensor and analyte occur rapidly. Grx1-roCherry is insensitive to $H_2O_2$ concentrations, even far beyond physiological values (500 μM). Under the same conditions, Grx1-roGFP2 develops a low-amplitude ratiometric response. Both biosensors are extremely sensitive to N-chlorotaurine, even at micromolar concentrations (10 μM). In contrast to the green biosensor, Grx1-roCherry responds to high (but likely nonphysiological) concentrations of NO generated by 100 μM MAHMA NONOate. Both probes demonstrate moderate sensitivity to the superoxide anion radical produced by the xanthine oxidase system (50 μM xanthine).

The midpoint redox potential of Grx1-roCherry was determined to be − 311 mV at pH 7.0 and − 335 mV at pH 7.4 (Fig. 3A). We also determined the value for Grx1-roGFP2 at our experimental conditions, which was − 291 mV at pH 7.0 and − 315 mV at pH 7.4 (Fig. 3B). Therefore, our estimation of Grx1-roGFP2 midpoint potential is slightly lower compared to the literature (− 280 mV) with a difference of about 10 mV. The value of − 311 mV for Grx1-roCherry is consistent with other data, namely with total oxidation of the probe in the lumen of the ER or titration by $H_2O_2$ in HeLa Kyoto cells (Fig. 3C) where inflection point of the Grx1-roCherry curve is located to the left of the Grx1-roGFP2 one indicating that the red sensor is more susceptible to oxidation.

### 3.3. Direct comparison of Grx1-roCherry and Grx1-roGFP2 coexpressed in the same cells

We tested whether Grx1-roCherry and Grx1-roGFP2 can be coexpressed and function in the same cells. HeLa Kyoto cells were transfected with cytosolic versions of the biosensors, and the plasmids for transfection were mixed to a 1:1 ratio. The fluorescent signal of the cells was observed the next day after transfection using a confocal microscope with standard imaging parameters for these proteins. We found many cells within which the red and green signals were distributed evenly. We next compared the sensitivity of Grx1-roCherry and Grx1-roGFP2 to oxidation by expressing cytosolic biosensors in cells plated on μ-slides (Ibidi). The advantage of these slides is that the medium volume inside the channel is small can be replaced very quickly. We added medium with a different concentration of $H_2O_2$ and observed changes in the signals of red and green biosensors in the same cells for several minutes. The dynamic range of Grx1-roGFP2 is much higher than for Grx1-roCherry. Thus, the signal of the green biosensor ($F_{405}$/$F_{488}$) under its maximum oxidation increased 6-fold, while the red signal ($F_{559}$) under the same conditions did not change more than 1.8-fold. However, the two biosensors were comparable in their sensitivity (Fig. 3C). Given that our *in vitro* data demonstrate that Grx1-roCherry is not able to directly sense $H_2O_2$ concentrations used in these experiments (Fig. 2C), we assume that, similar to Grx1-roGFP2, the probe responds to $H_2O_2$-driven 2GSH/GSSG ratio change in the cells.

### 3.4. 2-AAPA inhibitor blocks the function of Grx1-roCherry and Grx1-roGFP2

In work devoted to the development of the rxRFP biosensor, the authors tested the effectiveness of the biosensor in cells by inhibiting glutathione reductase (GR) [27]. The inhibitor was 2-AAPA (2-acetylamino-3-[4-(2-acetylamino-2-carboxyethylsulfanylthiocarbonylamino)phenylthiocarbamoylsulfanyl]

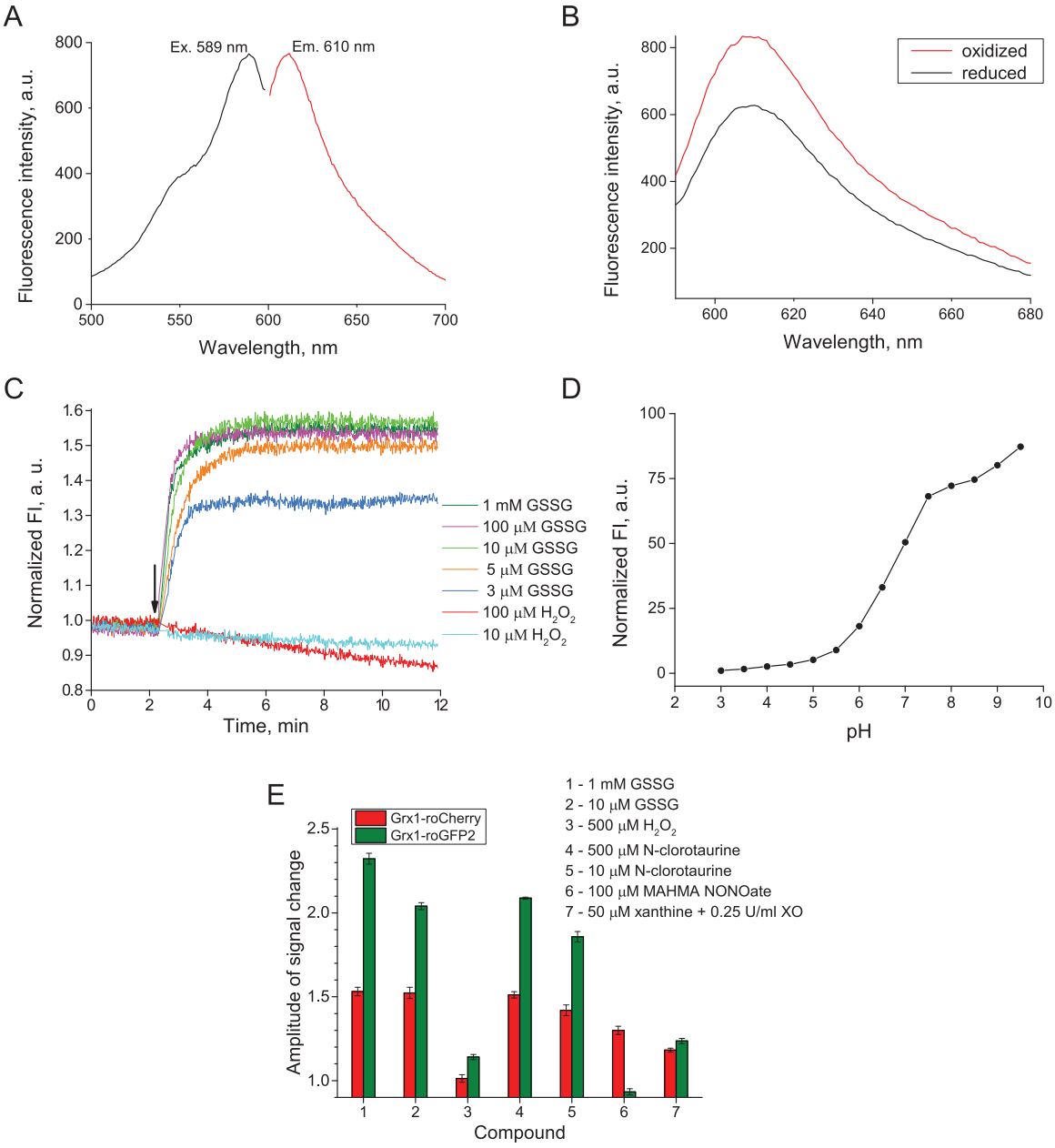


**Fig. 2.** Characterization of Grx1-roCherry biosensor. (A) Excitation and emission spectra of purified Grx1-roCherry. (B) Emission spectrum of 40 nM Grx1-roCherry in PBS (pH 7.4) in reduced form (with 1 mM GSH, 2 mM NADPH, 0.5–1.5 U/ml glutathione reductase) and oxidized form (with 1 mM GSSG). Excitation at 577 nm. (C) Changes in Grx1-roCherry fluorescence intensity in the presence of different GSSG and $H_2O_2$ concentrations as a function of time. All lines were normalized to values obtained from an intact protein sample incubated at the same conditions to eliminate component of atmosphere oxygen-driven oxidation. The moment of GSSG or $H_2O_2$ addition is marked with an arrow. The total volume of the sample is 1 ml with protein concentration of 40 nM (PBS, pH = 7.4). (D) pH dependency of purified reduced Grx1-roCherry. (E) Amplitude of signal change of reduced Grx1-roCherry ($F_{589}$) and Grx1-roGFP2 ($F_{405}/F_{488}$) responding to various oxidants. Incubation time was 3 min for samples 1–5 and 10 min for samples 6–7. Error bars indicate standard error of mean from 3 experiments.

propionic acid). When the cells were incubated with 200 μM 2-AAPA, rxRFP demonstrated oxidation in the cytoplasm [27]. In another series of experiments, the rxRFP-based TrxRFP1 biosensor used to monitor the thioredoxin redox state was coexpressed with Grx1-roGFP2 in the same cells. The addition of 2-AAPA to these cells led to oxidation of Grx1-roGFP2 at high concentrations of inhibitor, and the TrxRFP1 biosensor was also oxidized [34].

To reproduce these data with Grx1-roCherry, we coexpressed cytosolic Grx1-roCherry and mitochondria-targeted Grx1-roGFP2 (Grx1-roGFP2-mito) in HeLa Kyoto cells. The addition of 2-AAPA in a concentration of 100 μM to the cells led to a decrease in green signal ($F_{488}$) in the mitochondria, which corresponds to oxidation. However, we also observed a simultaneous decrease in the intensity of red fluorescence in the cytoplasm, which corresponds to a reduction in Grx1-roCherry under the same conditions. In attempts to explain such a controversial result, we found that both biosensors lose their activity after the incubation of cells with 2-AAPA. The signal from both biosensors changed irreversibly, and neither Grx1-roCherry nor Grx1-roGFP2 retained the ability to react to the cellular glutathione oxidation caused by the addition of $H_2O_2$ (Fig. 3D). We assumed that the effect of the inhibitor induced a nonspecific response in the biosensors. Our hypothesis was confirmed by previously obtained experimental data, indicating that 2-AAPA irreversibly inhibits Grx1 in a time- and concentration-dependent manner [35]. Thus, 2-AAPA should not be used in systems involving

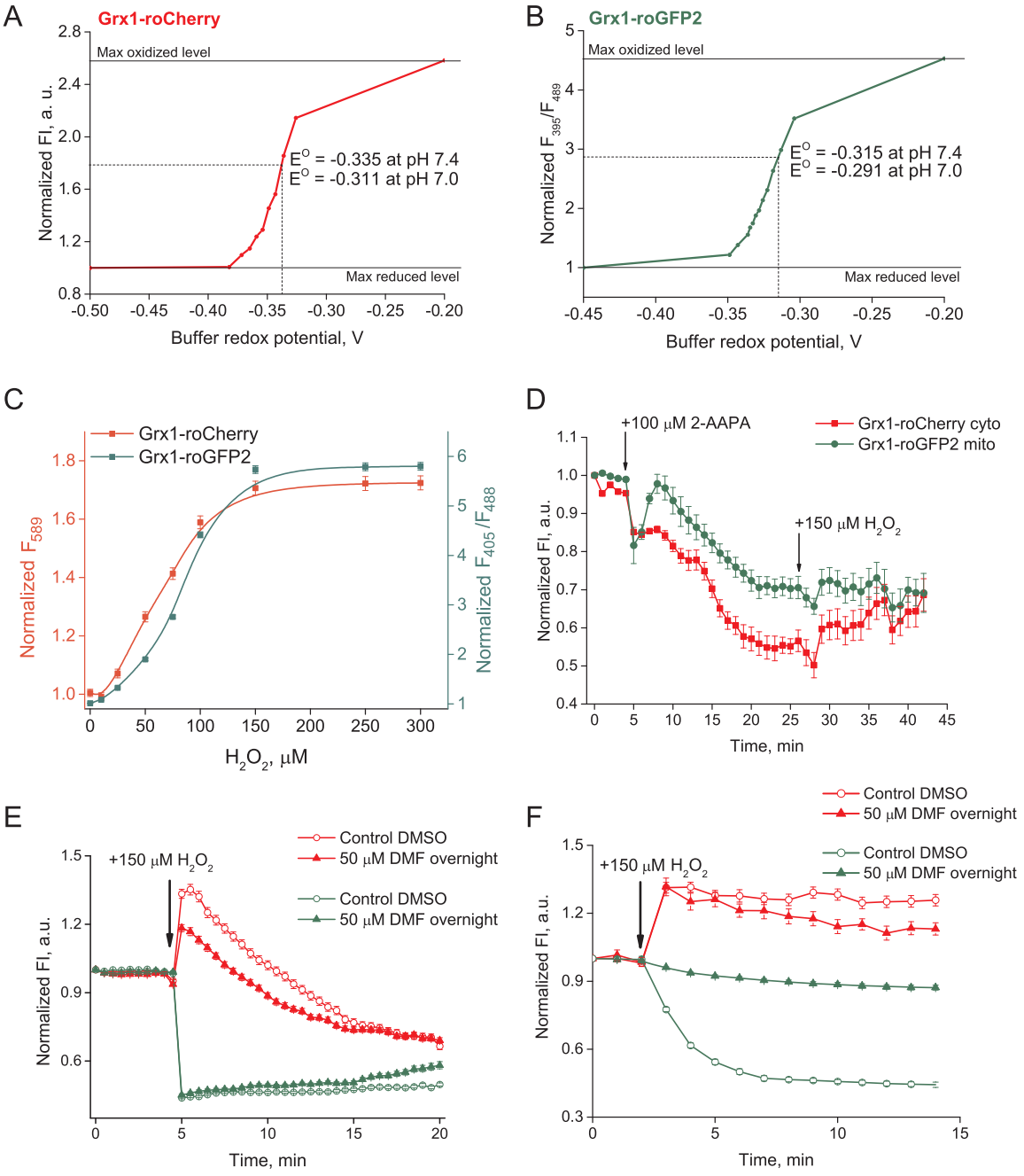


**Fig. 3.** Redox equilibria of Grx1-roCherry (A) and Grx1-roGFP2 (B) by titration against DTT. The total concentration of $DTT_{red}$ and $DTT_{ox}$ is 1 mM. Probes were incubated for 3 h at room temperature. All buffers shared a pH value of 7.4. (C) Redox titration of Grx1-roCherry ($F_{589}$) and Grx1-roGFP2 ($F_{405}/F_{488}$) coexpressed in cytoplasm of HeLa Kyoto cells. The dynamics of both biosensors were imaged in real time. Sensors reached the maximum level of response range within a few seconds after addition of $H_2O_2$. Error bars indicate standard error of mean from 3 experiments. (D) The dynamics of Grx1-roCherry ($F_{589}$ signal) and Grx1-roGFP2 ($F_{488}$ signal) in response to exogenous addition of 100 μM 2-AAPA (inhibitor of GR). Grx1-roCherry and Grx1-roGFP2 were coexpressed in HeLa Kyoto cells in cytoplasm and mitochondria, respectively. The functional activity of the biosensors was examined by addition of 150 μM $H_2O_2$. Signal values of Grx1-roCherry and Grx1-roGFP2 were normalized to the initial values. Signals were averaged from 32 cells in 2 experiments. Error bars indicate standard error of mean. (E) Fluorescence dynamics in HeLa Kyoto cells expressing Grx1-roCherry in the cytoplasm ($F_{589}$ signal, red line) and Grx1-roGFP2 in mitochondria ($F_{488}$ signal, green line) exposed to external $H_2O_2$. Cells were pretreated with either 50 μM DMF for 24 h or DMSO as the negative control. Signal values of Grx1-roCherry and Grx1-roGFP2 were normalized to the initial value. Signals were averaged from 103 cells in 3 experiments with DMF; from 119 cells in 3 experiments with DMSO. Error bars indicate standard error of mean. (F) Experiment described in (E) with localization of Grx1-roCherry in mitochondria ($F_{589}$ signal, red line) and Grx1-roGFP2 in cytoplasm ($F_{488}$ signal, green line). Signal values of Grx1-roCherry and Grx1-roGFP2 were normalized to the initial value. Signals were averaged from 30 cells in 2 experiments with DMF; from 34 cells in 2 experiments with DMSO. Error bars indicate standard error of mean. (For interpretation of the references to color in this figure legend, the reader is referred to the web version of this article).

biosensors, the function of which depends on glutaredoxins.

### 3.5. Dimethyl fumarate (DMF) makes cells less susceptible to oxidative stress

DMF has a cytoprotective effect, since it stimulates the synthesis of GSH. It is known that DMF activates nuclear factor (erythroid-derived 2)-like 2 (NRF2) and upregulates glutathione reductase [36]. We co-expressed Grx1-roCherry-cyto and Grx1-roGFP2-mito in HeLa Kyoto cells to detect changes in the redox states in the glutathione pool caused by incubation with DMF. According to literary sources, DMF causes a long-term cellular response, and therefore we incubated the cells with 50 μM DMF for 24 h. We then monitored the dynamics of oxidation of the glutathione pool in the cytoplasm and mitochondria after the addition of 150 μM $H_2O_2$. The response amplitude of Grx1-roCherry-cyto in cells incubated with DMF was significantly lower than in the cytoplasm of the control cells (without DMF). This means that the biosensor in the DMF-treated cells is oxidized less effectively. In mitochondria, the signal of Grx1-roGFP2-mito in the cells treated with DMF changed identically in response to oxidation in comparison with untreated cells. However, we observed faster dynamics of the subsequent reduction of the mitochondrial glutathione pool in cells incubated with DMF (Fig. 3E). Thus, DMF does have a greater reducing effect on the intracellular environment.

To exclude the possibility that the effect caused by DMF resulted from different properties of Grx1-roGFP2 and Grx1-roCherry, we repeated this experiment, but this time the red biosensor was localized in the mitochondria and the green biosensor was localized in the cytoplasm. However, we obtained a similar result. In the mitochondria of the DMF-treated and control cells, Grx1-roCherry demonstrated a similar response amplitude after addition of $H_2O_2$. However, in the cells incubated with DMF, we, as before, observed faster dynamics of the reduction in mitochondria. As in the previous experiment, the greatest difference was observed in the cytoplasm of cells. Judging by the dynamics of Grx1-roGFP2, the cytoplasmic glutathione pool is oxidized less effectively in cells after treatment with DMF (Fig. 3F). Grx1-roCherry in the cytoplasm of the DMF-treated cells demonstrated slightly larger response amplitude compared to the control. This can be explained by more negative value of the midpoint redox potential of Grx1-roCherry. However, in this series of experiments, biosensors showed similar response dynamics in different compartments.

### 3.6. Change in 2GSH/GSSG ratio during hypoxia and subsequent reoxygenation

It has been demonstrated that hypoxia/reoxygenation induces extensive ROS production in cells [37]. Would this condition also affect the GSH/GSSG ratio? To test this, HeLa Kyoto cells expressing Grx1-roCherry-cyto and Grx1-roGFP2-mito were subjected to hypoxia (0% oxygen) during fluorescence microscopy for 20 min. Grx1-roCherry-cyto did not demonstrate significant changes in the glutathione pool in the cytoplasm. At the same time, a powerful reduction during hypoxia was observed in the mitochondria (Fig. 4A). After hypoxia, the oxygen level in the chamber was returned to the normal state (21%). We observed that in this system, reoxygenation led to pronounced oxidation in the mitochondrial matrix (Fig. 4A); however, the cytosolic GSH pool remained stable. This is consistent with the observation that hypoxia-reoxygenation mostly affects mitochondria, leading to ROS production by reverse electron transport in the electron transport chain [38], and with studies demonstrating that the cytosolic GSH pool is much more stable than the mitochondrial pool [39].

### 3.7. Aerobic glycolysis to oxphos transition has different effects on the redox state of HeLa Kyoto and HEK293 cells

The metabolism of many cancer cells is more dependent on glycolysis, even in the presence of oxygen. This phenomenon is known as aerobic glycolysis or the Warburg effect [40,41]. The shifting metabolism of cancer cells from aerobic glycolysis to oxidative phosphorylation by mitochondria is considered one approach to treat cancer. One hypothesis is that cancer cells are very sensitive to oxidative stress and avoid the active respiration associated with elevated ROS production [42,43].

DCA is an example of a compound that switches the metabolism of cancer cells from glycolysis to oxidative phosphorylation [44]. The mechanism of action of DCA is based on the activation of the pyruvate dehydrogenase complex through the inhibition of pyruvate dehydrogenase kinase. However, the mechanism by which the switch from aerobic glycolysis to oxphos affects redox parameters in the cell remains unknown.

To investigate how DCA affects the most important redox parameters, such as 2GSH/GSSG and $NAD^+$/NADH, in HeLa Kyoto cells we have coexpressed in these cells Grx1-roCherry-cyto and the green-emitting biosensor SoNar [16] for the $NAD^+$/NADH ratio. The cells were incubated in media containing 30 mM DCA for 48 h. Then, flow cytometry was used to analyze the distribution of fluorescent signals in cell populations. It turned out that incubation of cells with DCA does lead to oxidation of the cytoplasmic pool of glutathione and reduction of the NAD pool compared to cells without addition of the substance (Fig. 4B). Oxidation of glutathione could be explained by enhanced mitochondrial activity, but a lower $NAD^+$/NADH ratio could be due to a lower flux of pyruvate towards lactate in the reaction catalyzed by lactate dehydrogenase.

Notably, we conducted the same experiment with HEK293 cells, which are noncancerous immortalized human cells, and we did not observe any redox changes during incubation with DCA in these cells (Fig. 4C). In addition, using the pH biosensor SypHer2 [45], we made sure that DCA does not cause significant changes in cytosolic pH that could affect the signal of SoNar and, to lesser extent, Grx1-roCherry. Probably, the switch from aerobic glycolysis to oxidative phosphorylation can induce a pro-oxidative shift in cancer HeLa Kyoto cells, in contrast to nontumor HEK293 cells. Given the high sensitivity of cancer cells to oxidative stress [42,46] compared to normal cells, compounds promoting pyruvate transport into the matrix could be essential components of anticancer redox therapies. However, to verify this assumption, future studies are required with a greater number of different types of cell lines.

### 3.8. Localized generation of $H_2O_2$ revealed differences in dynamics of the 2GSH/GSSG ratio in cellular compartments of different cell types

Hydrogen peroxide production is a main factor in glutathione oxidation under oxidative stress conditions. However, how compartment-specific $H_2O_2$ generation affects the 2GSH/GSSG ratio in other compartments remains unknown.

To answer this question, we used D-amino-acid oxidase (DAO), an enzyme that oxidizes various D-amino acids and generates $H_2O_2$ as a reaction product [47]. DAO is an efficient genetically encoded tool capable of substrate-controlled $H_2O_2$ generation in various organelles [48,49].

In our experiments, we generated $H_2O_2$ in the nucleus and in the mitochondrial matrix using the localized DAO versions, DAO-NLS and DAO-mito, respectively, and monitored GSH/GSSG ratio dynamics in the cytoplasm and mitochondria using Grx1-roCherry-cyto and Grx1-roGFP2-mito. In addition, we used two different cell types: primary mouse cortical neurons and HeLa Kyoto cells. DAO-generated $H_2O_2$ in these cells was induced by adding DAO substrate, 2 mM D-norvaline, to the cell culture medium.

We found that generation of $H_2O_2$ in the nucleus causes oxidation of the glutathione pool in the mitochondria and in the cytoplasm of both cell types (Fig. 5A, B). In neurons, Grx1-roCherry-cyto and Grx1-roGFP2-mito also demonstrate the oxidation of glutathione in both

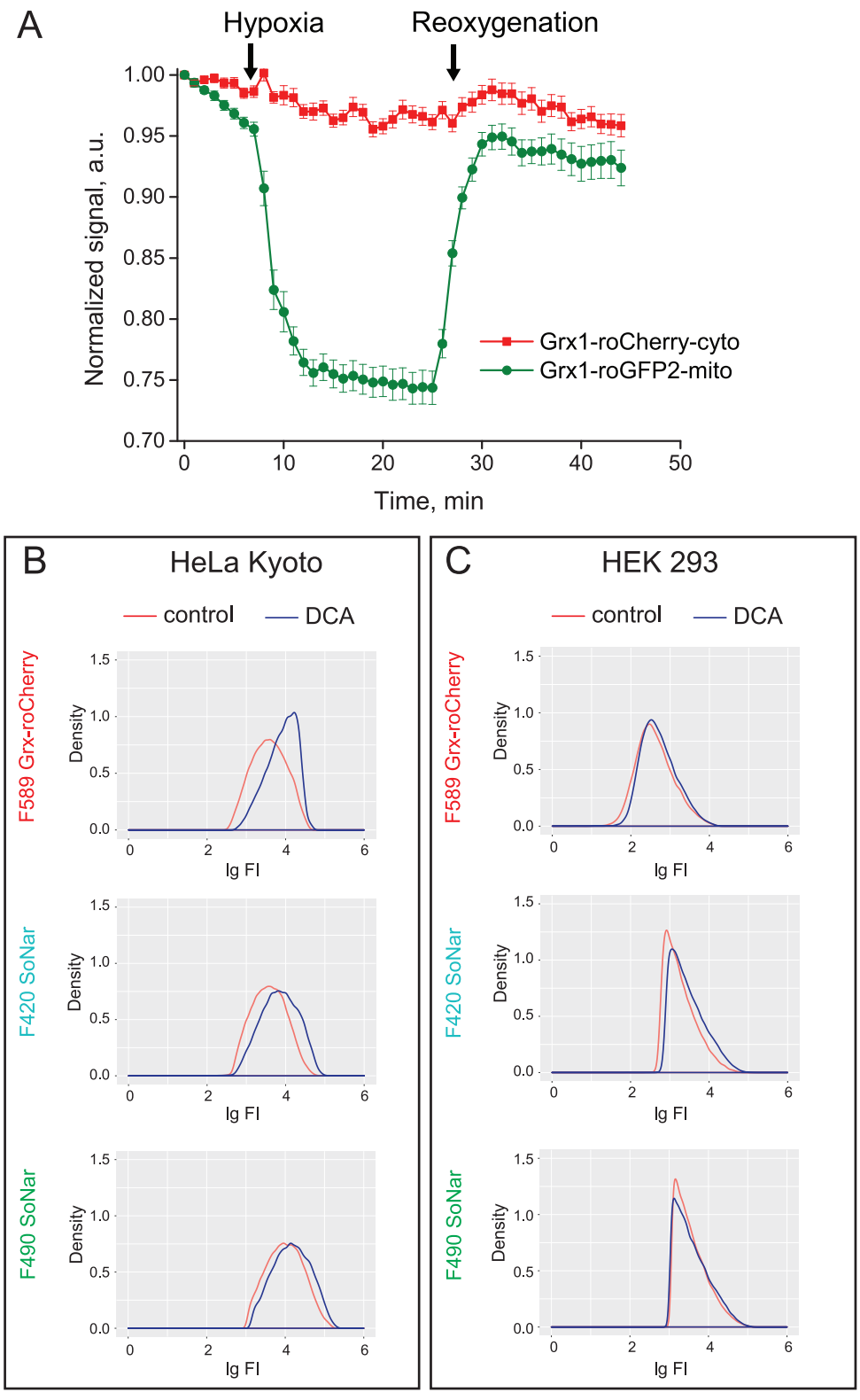


**Fig. 4.** (A) HeLa Kyoto cells coexpressing Grx1-roCherry in cytoplasm ($F_{589}$ signal, red line) and Grx1-roGFP2 in mitochondria ($F_{405}/F_{488}$ signal, green line) were exposed to hypoxia, with subsequent reoxygenation. Signal values of Grx1-roCherry and Grx1-roGFP2 were normalized to the initial value. Signals were averaged from 28 cells in 2 experiments. Error bars indicate standard error of mean. (B) HeLa Kyoto cells coexpressing Grx1-roCherry and SoNar in cytoplasm were analyzed by flow cytometry after incubation with 30 mM DCA for 48 h (shown in blue) in comparison with untreated cells (shown in red). For each graph 10,000 cells were analyzed. (C) Experiment described in (B) with HEK293 cells. (For interpretation of the references to color in this figure legend, the reader is referred to the web version of this article).

compartments when $H_2O_2$ is produced in the mitochondrial matrix (Fig. 5C). However, in HeLa Kyoto cells, only the mitochondrial glutathione pool is oxidized upon mitochondrial $H_2O_2$ production (Fig. 5D).

Antioxidant systems of cancer cells are highly effective. However, most tumor cells are more dependent on a Trx system [50,51]. In particular, TrxR and Trx are overexpressed in many such pathological cells. For this reason, the Trx system, mainly TrxR, is considered one of the main targets for the development of new anticancer drugs [52]. We repeated the previous experiment with HeLa Kyoto cells in the presence of auranofin, a potent TrxR system inhibitor [53]. We found that in HeLa Kyoto cells incubated overnight with 2.5 μM auranofin, the oxidation of the glutathione pool induced by the generation of $H_2O_2$ *via* DAO-mito was observed both in the mitochondria and in the cytoplasm (Fig. 5E). In control experiments, we incubated the cells with DMSO under the same conditions, since auranofin was dissolved in DMSO. In

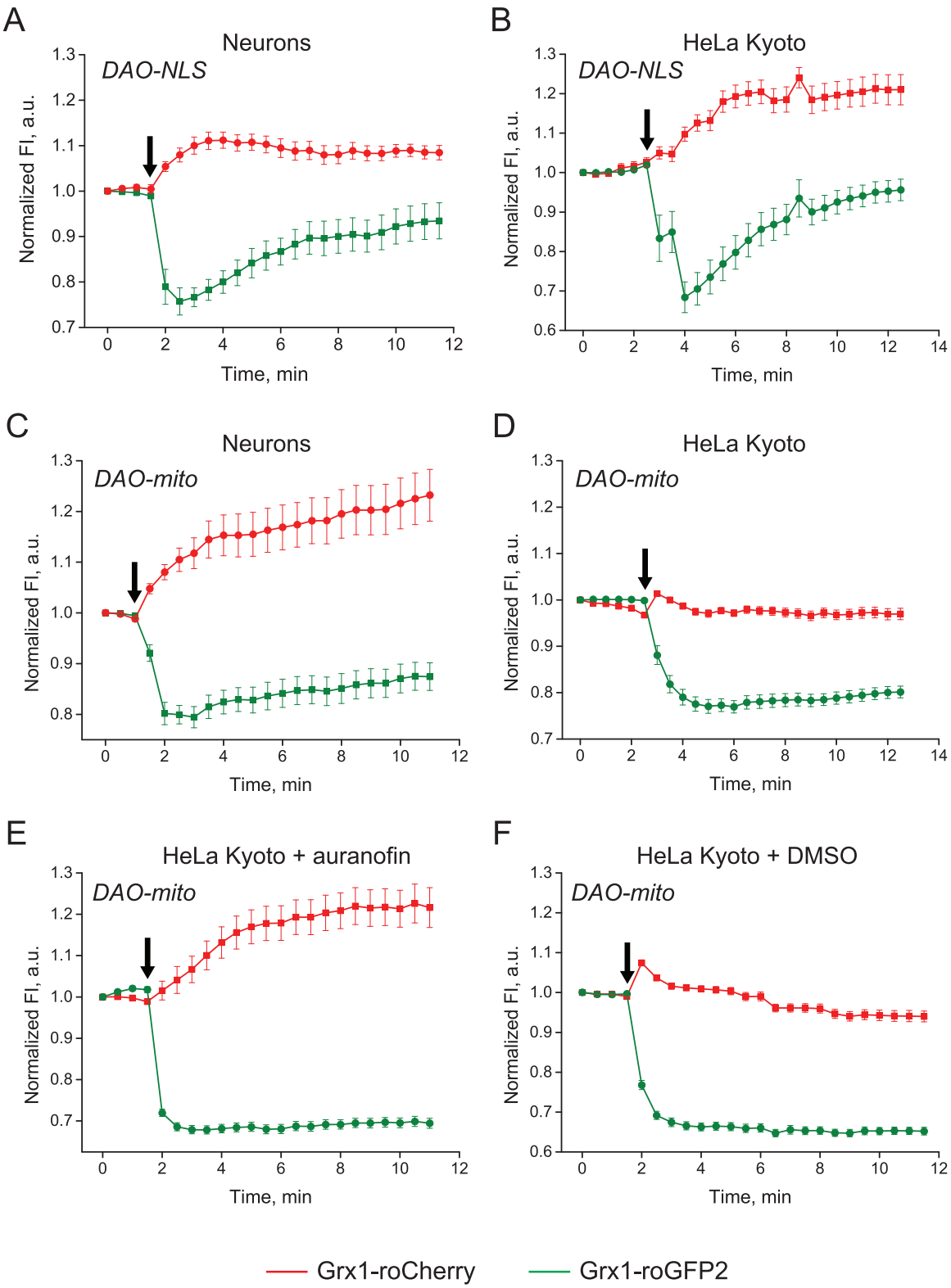


**Fig. 5.** Dynamics of glutathione redox state in cytosol (red line) and mitochondrial matrix (green line) caused by local generation of $H_2O_2$ by DAO in neurons and HeLa Kyoto cells. Neurons of mixed mouse primary embryonic cortex cell culture and HeLa Kyoto cells were cotransfected by cytosolic Grx1-roCherry ($F_{589}$ signal) and mitochondrial Grx1-roGFP2 ($F_{488}$ signal). In the same cells, DAO was localized to nuclei (A, B) or mitochondria (C-F). The arrows in all graphs indicate the start of inducible $H_2O_2$-generation in nuclei or mitochondria caused by the addition of 2 mM D-norvaline to the cell culture medium. To evaluate the effect of TrxR inhibition, HeLa Kyoto cells coexpressing Grx1-roCherry in cytoplasm, Grx1-roGFP2 and DAO in mitochondria were preincubated overnight with 2.5 μM auranofin (E) and DMSO (control probe) (F), followed by 2 mM D-norvaline treatment. In all graphs, error bars indicate standard error of mean. Signal values of Grx1-roCherry and Grx1-roGFP2 were normalized to the initial value. Signals in each series were averaged in 3 experiments from at least 11 neurons and 40 HeLa Kyoto cells. (For interpretation of the references to color in this figure legend, the reader is referred to the web version of this article).

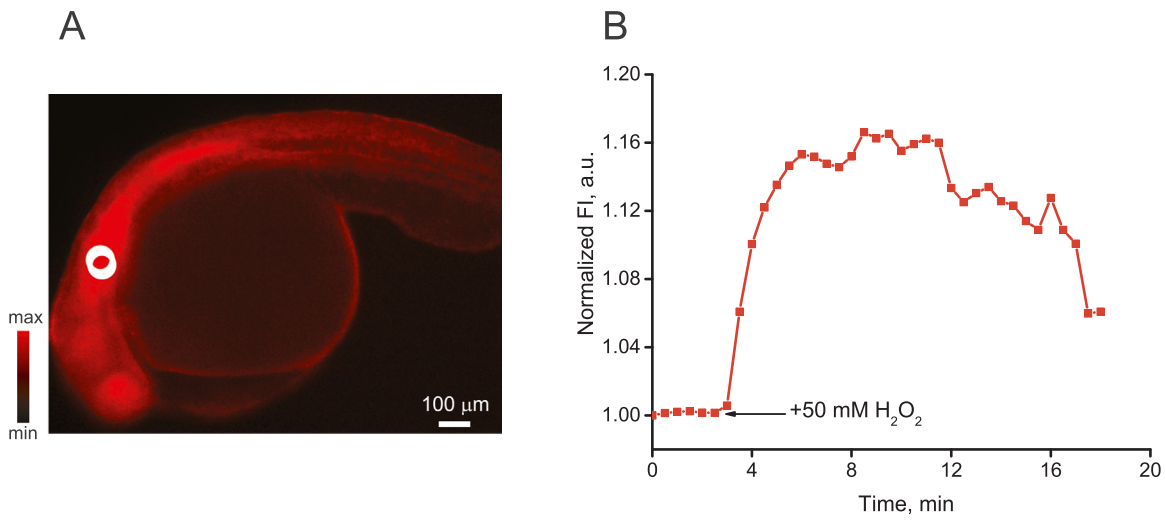


**Fig. 6.** Grx1-roCherry in tissues of zebrafish *D. rerio*. (A) Image of zebrafish larva at 48 h stage injected with mRNA encoding Grx1-roCherry. White ROI indicates area in which fluorescent signal was detected in (B). Scale bar 100 µM. Lookup table indicates intensity of red fluorescence. (B) Dynamics of Grx1-roCherry signal in the noted area (A) of fish tissue in response to oxidation caused by the exogenous addition of 50 mM $H_2O_2$.

this case, we still observed a change in the 2GSH/GSSG ratio in the mitochondria after the addition of D-norvaline (Fig. 5F). Thus, the Trx system does play a key role in the control of redox signals between cellular compartments.

### 3.9. Grx1-roCherry in zebrafish D. rerio

Finally, we tested Grx1-roCherry performance *in vivo* in the tissues of zebrafish *D. rerio*. To do this, we injected biosensor mRNA into the yolk of embryos at the stage of a single cell. On the second day, the fluorescent signal was imaged in animal tissues using a fluorescence microscope (Fig. 6A). Grx1-roCherry demonstrates the dynamics of glutathione oxidation in fish tissues caused by the addition of 50 mM $H_2O_2$ (Fig. 6B).

## 4. Discussion

We have developed a new redox-sensitive biosensor based on red FP mCherry (roCherry). roCherry significantly differs in the design of the construct from the previously developed biosensor rxRFP [27]. As with the classical proteins of this family, redox-active cysteines have been integrated into the structure of the protein β-barrel. Moreover, in contrast to rxRFP, roCherry contains human Grx1 at the N-terminus that is fused through a polypeptide linker. The principle of functioning of all roFPs is based on the fact that the redox-state of a pair of active cysteines is equilibrated with the cellular pool of glutathione, and this equilibration is catalyzed by Grxs. It was demonstrated for rxYFP and roGFP that fusion with Grx dramatically elevates the reaction speed of the probe [23,24]. One study involving Grx1-roGFP2 revealed that the oxidation of Grx1-roGFP2 by GSSG is at least 100,000 times faster than single roGFP2 [24]. In our work, we also confirmed that Grx1 is necessary for the function of Grx1-roCherry, since a single roCherry reacts to oxidation much more slowly. In addition, we tested whether Grx1 can be localized at the C-terminus of the construct. This information can be important when planning the development of fused or targeted versions.

The peculiarity of circularly permuted FPs is that they have a more flexible structure, but the chromophore itself is more influenced by the intracellular environment. Perhaps for this reason, a previously reported rxRFP is sensitive to oxidation by certain components, for example, peroxynitrite and superoxide anion radical [27]. However, the redox pair of active cysteines exposed to the outside in protein structures can be oxidized nonspecifically. In particular, we demonstrated *in vitro* that Grx1-roCherry and Grx1-roGFP2 are oxidized by chlorothaurine. Our data correlate with recently obtained results confirming that roGFP2-based probes can be oxidized by hypochlorite in cells and *in vitro* with fast kinetics [54,55]. In addition, Grx1-roCherry and Grx1-roGFP2 demonstrate a slight response to oxidation with superoxide anion radical. In addition, unlike Grx1-roGFP2, Grx1-roCherry demonstrates a response to the high concentration of nitric oxide generated by MAHMA NONOate. Thus, although all proteins in this family react mainly to 2GSH/GSSG ratio changes, the possibility of nonspecific oxidation should be considered.

The midpoint redox potential of Grx1-roCherry was determined to be − 311 mV at pH 7.0. For comparison, the midpoint potentials of roGFP1 (−291 mV), roGFP2 (−280 mV) and rxYFP (−261 mV) are more positive. All of these sensors have limitations on use in oxidizing compartments, such as the lumen of the endoplasmic reticulum (ER). That is because the redox potential of glutathione in the ER is approximately − 208 mV [56].

One main advantage of a red biosensor is that it can be used in combination with biosensors based on proteins emitting in the green portion of the visible spectrum. As mentioned earlier, the panel of existing biosensors mainly consists of green proteins. In our work, we tested the function of the new biosensor Grx1-roCherry in various systems, in combination with some popular green-emitted biosensors such as Grx1-roGFP2, SoNar, and SypHer2. The multiparameter imaging mode is more informative, since it allows monitoring of changes in several intracellular parameters simultaneously. For example, this approach allows study of the dynamics of the same processes in various cellular compartments. In particular, using redox-sensitive biosensors, we confirmed that the dynamics of the redox state of the glutathione pool in the cytoplasm and mitochondria can differ substantially. A bright example is the model of hypoxia-reoxygenation, which demonstrates global changes in the 2GSH/GSSG ratio in the matrix of mitochondria, while the redox state of the cytoplasmic pool does not change significantly. The respiratory chain of mitochondria is the main consumer of reducing equivalents. Therefore, with hypoxia, when the mitochondrial respiratory chain is turned off, the mitochondrial matrix is further reduced. Reoxygenation induces oxidation associated with the formation of ROSs by an electron transport chain.

The metabolism and redox state of cells largely depends on their type. For example, we observed that DCA, an activator of the pyruvate dehydrogenase complex, causes changes in the redox state of cancer HeLa Kyoto cells, which predominantly use aerobic glycolysis. At the same time, HEK293 cells that mainly employ oxidative respiration do

not demonstrate similar dynamics during DCA treatment. This system serves as a clear example of the effectiveness of biosensors for screening drugs that specifically affect the metabolism of pathological cells.

Finally, we tested Grx1-roCherry in the tissues of the zebrafish *D. rerio*. We ensured that the biosensor functions in this system and reacts to a change in the 2GSH/GSSG ratio. In addition, the bright red fluorescence signal of this biosensor is well detectable in tissues. The main disadvantage of Grx1-roCherry in this system is the intensiometric character of the readout. This protein has a single peak in the excitation and emission spectra of fluorescence. Intensiometric readouts depend on the expression level of protein in cells, which does not allow for quantitative evaluation of the investigated parameter in the 2GSH/GSSG ratio. In complex research objects, such as fish, additional measurement artifacts can be caused by the movement of the object or by changing the shape of organs. Therefore, control experiments are essential in each study based on intensiometric biosensors, especially *in vivo* systems.

## 5. Conclusions

We have developed a new redox-sensitive biosensor, Grx1-roCherry, based on the red fluorescent protein mCherry and human glutaredoxin1. The protein was characterized *in vitro* and was successfully tested in various types of eukaryotic cells in the multiparametric imaging mode, in combination with other redox biosensors.

## Acknowledgements

We thank Robert Campbell for mCherry, Tobias Dick for Grx1-roGFP2, and Yi Yang for SoNar expression vectors. Experiments were partially carried out using the equipment provided by the IBCH core facility (CKP IBCH, supported by Russian Ministry of Education and Science, Grant RFMEFI62117X0018).

The work was supported by Russian Science Foundation grant 17-15-01175 (to D.S.B) and Deutsche Forschungsgemeinschaft DFG, IRTG 1816 (to D.K and V.V.B).

Chapter “Grx1-roCherry in zebrafish *D. rerio*” was supported by the Russian Foundation for Basic Research grant 16-34-60175 (to D.S.B).

## Author disclosure statement

No competing financial interests exist.

## References

[1] C.H. Lillig, C. Berndt, A. Holmgren, Glutaredoxin systems, Biochim. Biophys. Acta 1780 (2008) 1304–1317, https://doi.org/10.1016/j.bbagen.2008.06.003.

[2] A.P. Fernandes, A. Holmgren, Glutaredoxins: glutathione-dependent redox enzymes with functions far beyond a simple thioredoxin backup system, Antioxid. Redox Signal. 6 (2004) 63–74, https://doi.org/10.1089/152308604771978354.

[3] M. Deponte, Glutathione catalysis and the reaction mechanisms of glutathione-dependent enzymes, Biochim. Biophys. Acta 1830 (2013) 3217–3266, https://doi.org/10.1016/j.bbagen.2012.09.018.

[4] J. Sedlak, R.H. Lindsay, Estimation of total, protein-bound, and nonprotein sulfhydryl groups in tissue with Ellman's reagent, Anal. Biochem. 25 (1968) 192–205.

[5] X. Jiang, Y. Yu, J. Chen, M. Zhao, H. Chen, X. Song, A.J. Matzuk, S.L. Carroll, X. Tan, A. Sizovs, N. Cheng, M.C. Wang, J. Wang, Quantitative imaging of glutathione in live cells using a reversible reaction-based ratiometric fluorescent probe, ACS Chem. Biol. 10 (2015) 864–874, https://doi.org/10.1021/cb500986w.

[6] X. Jiang, J. Chen, A. Bajic, C. Zhang, X. Song, S.L. Carroll, Z.L. Cai, M. Tang, M. Xue, N. Cheng, C.P. Schaaf, Quantitative real-time imaging of glutathione, 2017, 8, p. 16087, published online EpubJul 13 ⟨http://dx.doi.org/10.1038/ncomms16087⟩.

[7] D.S. Bilan, V.V. Belousov, New tools for redox biology: from imaging to manipulation, Free Radic. Biol. Med. 109 (2017) 167–188, https://doi.org/10.1016/j.freeradbiomed.2016.12.004.

[8] V.V. Belousov, A.F. Fradkov, K.A. Lukyanov, D.B. Staroverov, K.S. Shakhbazov, A.V. Terskikh, S. Lukyanov, Genetically encoded fluorescent indicator for intracellular hydrogen peroxide, Nat. Methods 3 (2006) 281–286, https://doi.org/10.1038/nmeth866.

[9] K.N. Markvicheva, D.S. Bilan, N.M. Mishina, A.Y. Gorokhovatsky, L.M. Vinokurov, S. Lukyanov, V.V. Belousov, A genetically encoded sensor for H2O2 with expanded dynamic range, Bioorg. Med. Chem. 19 (2011) 1079–1084, https://doi.org/10.1016/j.bmc.2010.07.014.

[10] D.S. Bilan, L. Pase, L. Joosen, A.Y. Gorokhovatsky, Y.G. Ermakova, T.W. Gadella, C. Grabher, C. Schultz, S. Lukyanov, V.V. Belousov, HyPer-3: a genetically encoded H(2)O(2) probe with improved performance for ratiometric and fluorescence lifetime imaging, ACS Chem. Biol. 8 (2013) 535–542, https://doi.org/10.1021/cb300625g.

[11] Y.G. Ermakova, D.S. Bilan, M.E. Matlashov, N.M. Mishina, K.N. Markvicheva, O.M. Subach, F.V. Subach, I. Bogeski, M. Hoth, G. Enikolopov, V.V. Belousov, Red fluorescent genetically encoded indicator for intracellular hydrogen peroxide, Nat. Commun. 5 (2014) 5222, https://doi.org/10.1038/ncomms6222.

[12] D.S. Bilan, V.V. Belousov, HyPer family probes: state of the art, Antioxid. Redox Signal. (2016), https://doi.org/10.1089/ars.2015.6586.

[13] Y.P. Hung, J.G. Albeck, M. Tantama, G. Yellen, Imaging cytosolic NADH-NAD(+) redox state with a genetically encoded fluorescent biosensor, Cell Metab. 14 (2011) 545–554, https://doi.org/10.1016/j.cmet.2011.08.012.

[14] Y. Zhao, J. Jin, Q. Hu, H.M. Zhou, J. Yi, Z. Yu, L. Xu, X. Wang, Y. Yang, J. Loscalzo, Genetically encoded fluorescent sensors for intracellular NADH detection, Cell Metab. 14 (2011) 555–566, https://doi.org/10.1016/j.cmet.2011.09.004.

[15] D.S. Bilan, M.E. Matlashov, A.Y. Gorokhovatsky, C. Schultz, G. Enikolopov, V.V. Belousov, Genetically encoded fluorescent indicator for imaging NAD(+)/NADH ratio changes in different cellular compartments, Biochim. Biophys. Acta 1840 (2014) 951–957, https://doi.org/10.1016/j.bbagen.2013.11.018.

[16] Y. Zhao, Q. Hu, F. Cheng, N. Su, A. Wang, Y. Zou, H. Hu, X. Chen, H.M. Zhou, X. Huang, K. Yang, Q. Zhu, X. Wang, J. Yi, L. Zhu, X. Qian, L. Chen, Y. Tang, J. Loscalzo, Y. Yang, SoNar, a Highly responsive NAD+/NADH sensor, allows high-throughput metabolic screening of anti-tumor agents, Cell Metab. 21 (2015) 777–789, https://doi.org/10.1016/j.cmet.2015.04.009.

[17] W.D. Cameron, C.V. Bui, A. Hutchinson, P. Loppnau, S. Graslund, J.V. Rocheleau, Apollo-NADP(+): a spectrally tunable family of genetically encoded sensors for NADP(+), Nat. Methods 13 (2016) 352–358, https://doi.org/10.1038/nmeth.3764.

[18] R. Tao, Y. Zhao, H. Chu, A. Wang, J. Zhu, X. Chen, Y. Zou, M. Shi, R. Liu, N. Su, J. Du, H. M. Zhou, L. Zhu, X. Qian, H. Liu, J. Loscalzo, Y. Yang, Genetically encoded fluorescent sensors reveal dynamic regulation of NADPH metabolism, 2017, 14, pp. 720-728, published online EpubJul ⟨http://dx.doi.org/10.1038/nmeth.4306⟩.

[19] H. Ostergaard, A. Henriksen, F.G. Hansen, J.R. Winther, Shedding light on disulfide bond formation: engineering a redox switch in green fluorescent protein, EMBO J. 20 (2001) 5853–5862, https://doi.org/10.1093/emboj/20.21.5853.

[20] G.T. Hanson, R. Aggeler, D. Oglesbee, M. Cannon, R.A. Capaldi, R.Y. Tsien, S.J. Remington, Investigating mitochondrial redox potential with redox-sensitive green fluorescent protein indicators, J. Biol. Chem. 279 (2004) 13044–13053, https://doi.org/10.1074/jbc.M312846200.

[21] C.T. Dooley, T.M. Dore, G.T. Hanson, W.C. Jackson, S.J. Remington, R.Y. Tsien, Imaging dynamic redox changes in mammalian cells with green fluorescent protein indicators, J. Biol. Chem. 279 (2004) 22284–22293, https://doi.org/10.1074/jbc.M312847200.

[22] M. Schwarzlander, T.P. Dick, A.J. Meyer, B. Morgan, Dissecting redox biology using fluorescent protein sensors, Antioxid. Redox Signal. 24 (2016) 680–712, https://doi.org/10.1089/ars.2015.6266.

[23] O. Bjornberg, H. Ostergaard, J.R. Winther, Mechanistic insight provided by glutaredoxin within a fusion to redox-sensitive yellow fluorescent protein, Biochemistry 45 (2006) 2362–2371, https://doi.org/10.1021/bi0522495.

[24] M. Gutscher, A.L. Pauleau, L. Marty, T. Brach, G.H. Wabnitz, Y. Samstag, A.J. Meyer, T.P. Dick, Real-time imaging of the intracellular glutathione redox potential, Nat. Methods 5 (2008) 553–559, https://doi.org/10.1038/nmeth.1212.

[25] A.I. Kostyuk, A.S. Panova, D.S. Bilan, V.V. Belousov, Redox biosensors in a context of multiparameter imaging, Free Radic. Biol. Med. (2018), https://doi.org/10.1016/j.freeradbiomed.2018.04.004.

[26] K. Sugiura, T. Nagai, M. Nakano, H. Ichinose, T. Nakabayashi, N. Ohta, T. Hisabori, Redox sensor proteins for highly sensitive direct imaging of intracellular redox state, Biochem. Biophys. Res. Commun. 457 (2015) 242–248, https://doi.org/10.1016/j.bbrc.2014.12.095.

[27] Y. Fan, Z. Chen, H.W. Ai, Monitoring redox dynamics in living cells with a redox-sensitive red fluorescent protein, Anal. Chem. 87 (2015) 2802–2810, https://doi.org/10.1021/ac5041988.

[28] Y. Zhao, S. Araki, J. Wu, T. Teramoto, Y.F. Chang, M. Nakano, A.S. Abdelfattah, M. Fujiwara, T. Ishihara, T. Nagai, R.E. Campbell, An expanded palette of genetically encoded Ca(2)(+) indicators, Science 333 (2011) 1888–1891, https://doi.org/10.1126/science.1208592.

[29] N. Koon, S.M. Yei, A.J. Risenmay, K. Kallio, S.J. Remington, I. Magpiong, Developing a redox-sensitive red fluorescent protein biosensor (S52-S52), J. Biomol. Tech. JBT 22 (2011) (S52-S52).

[30] N.C. Shaner, R.E. Campbell, P.A. Steinbach, B.N. Giepmans, A.E. Palmer, R.Y. Tsien, Improved monomeric red, orange and yellow fluorescent proteins derived from Discosoma sp. red fluorescent protein, Nat. Biotechnol. 22 (2004) 1567–1572, https://doi.org/10.1038/nbt1037.

[31] Y.P. Hung, G. Yellen, Live-cell imaging of cytosolic NADH-NAD+ redox state using a genetically encoded fluorescent biosensor, Methods Mol. Biol. 1071 (2014) 83–95, https://doi.org/10.1007/978-1-62703-622-1_7.

[32] W. Zhang, A.W. Lohman, Y. Zhuravlova, X. Lu, M.D. Wiens, H. Hoi, S. Yaganoglu, M.A. Mohr, Optogenetic control with a photocleavable protein, PhoCl 14 (2017) 391–394, https://doi.org/10.1038/nmeth.4222.

[33] A.J. Lam, F. St-Pierre, Y. Gong, J.D. Marshall, P.J. Cranfill, M.A. Baird, M.R. McKeown, J. Wiedenmann, M.W. Davidson, M.J. Schnitzer, R.Y. Tsien, M.Z. Lin, Improving FRET dynamic range with bright green and red fluorescent proteins, Nat. Methods 9 (2012) 1005–1012, https://doi.org/10.1038/nmeth.2171.

[34] Y. Fan, M. Makar, M.X. Wang, H.W. Ai, Monitoring thioredoxin redox with a genetically encoded red fluorescent biosensor, Nat. Chem. Biol. 13 (2017) 1045–1052, https://doi.org/10.1038/nchembio.2417.
[35] S.S. Sadhu, E. Callegari, Y. Zhao, X. Guan, T. Seefeldt, Evaluation of a dithiocarbamate derivative as an inhibitor of human glutaredoxin-1, J. Enzym. Inhib. Med. Chem. 28 (2013) 456–462, https://doi.org/10.3109/14756366.2011.649267.
[36] C. Hoffmann, M. Dietrich, A.K. Herrmann, T. Schacht, P. Albrecht, Dimethyl Fumarate Induces Glutathione Recycling by Upregulation of Glutathione Reductase, 2017, p. 6093903. ⟨http://dx.doi.org/10.1155/2017/6093903⟩.
[37] C. Li, R.M. Jackson, Reactive species mechanisms of cellular hypoxia-reoxygenation injury, Am. J. Physiol. Cell Physiol. 282 (2002) C227–241, https://doi.org/10.1152/ajpcell.00112.2001.
[38] E.T. Chouchani, V.R. Pell, E. Gaude, D. Aksentijevic, S.Y. Sundier, E.L. Robb, A. Logan, S.M. Nadtochiy, E.N.J. Ord, A.C. Smith, F. Eyassu, R. Shirley, C.H. Hu, A.J. Dare, A.M. James, S. Rogatti, R.C. Hartley, S. Eaton, A.S.H. Costa, P.S. Brookes, S.M. Davidson, M.R. Duchen, K. Saeb-Parsy, M.J. Shattock, A.J. Robinson, L.M. Work, C. Frezza, T. Krieg, M.P. Murphy, Ischaemic accumulation of succinate controls reperfusion injury through mitochondrial ROS, Nature 515 (2014) 431–435, https://doi.org/10.1038/nature13909.
[39] S.C. Albrecht, A.G. Barata, J. Grosshans, A.A. Teleman, T.P. Dick, In vivo mapping of hydrogen peroxide and oxidized glutathione reveals chemical and regional specificity of redox homeostasis, Cell Metab. 14 (() (2011) 819–829, https://doi.org/10.1016/j.cmet.2011.10.010.
[40] M.V. Liberti, J.W. Locasale, The Warburg effect: how does it benefit cancer cells? Trends Biochem. Sci. 41 (2016) 211–218, https://doi.org/10.1016/j.tibs.2015.12.001.
[41] M.G. Vander Heiden, L.C. Cantley, C.B. Thompson, Understanding the Warburg effect: the metabolic requirements of cell proliferation, Science 324 (2009) 1029–1033, https://doi.org/10.1126/science.1160809.
[42] M. Diehn, R.W. Cho, N.A. Lobo, T. Kalisky, M.J. Dorie, A.N. Kulp, D. Qian, J.S. Lam, L.E. Ailles, M. Wong, B. Joshua, M.J. Kaplan, I. Wapnir, F.M. Dirbas, G. Somlo, C. Garberoglio, B. Paz, J. Shen, S.K. Lau, S.R. Quake, J.M. Brown, I.L. Weissman, M.F. Clarke, Association of reactive oxygen species levels and radioresistance in cancer stem cells, Nature 458 (2009) 780–783, https://doi.org/10.1038/nature07733.
[43] V. Sosa, T. Moline, R. Somoza, R. Paciucci, H. Kondoh, L.L. ME, Oxidative stress and cancer: an overview, Ageing Res. Rev. 12 (2013) 376–390, https://doi.org/10.1016/j.arr.2012.10.004.
[44] S. Bonnet, S.L. Archer, J. Allalunis-Turner, A. Haromy, C. Beaulieu, R. Thompson, C.T. Lee, G.D. Lopaschuk, L. Puttagunta, S. Bonnet, G. Harry, K. Hashimoto, C.J. Porter, M.A. Andrade, B. Thebaud, E.D. Michelakis, A mitochondria-K+ channel axis is suppressed in cancer and its normalization promotes apoptosis and inhibits cancer growth, Cancer Cell 11 (2007) 37–51, https://doi.org/10.1016/j.ccr.2006.10.020.
[45] M.E. Matlashov, Y.A. Bogdanova, G.V. Ermakova, N.M. Mishina, Y.G. Ermakova, E.S. Nikitin, P.M. Balaban, S. Okabe, S. Lukyanov, G. Enikolopov, A.G. Zaraisky, V.V. Belousov, Fluorescent ratiometric pH indicator SypHer2: applications in neuroscience and regenerative biology, Biochim. Biophys. Acta 1850 (2015) 2318–2328, https://doi.org/10.1016/j.bbagen.2015.08.002.
[46] C. Gorrini, I.S. Harris, T.W. Mak, Modulation of oxidative stress as an anticancer strategy, Nat. Rev. Drug Discov. 12 (2013) 931–947, https://doi.org/10.1038/nrd4002.
[47] L. Pollegioni, K. Diederichs, G. Molla, S. Umhau, W. Welte, S. Ghisla, M.S. Pilone, Yeast D-amino acid oxidase: structural basis of its catalytic properties, J. Mol. Biol. 324 (2002) 535–546.
[48] Y.A. Bogdanova, C. Schultz, V.V. Belousov, Local generation and imaging of hydrogen peroxide in living cells, Curr. Protoc. Chem. Biol. 9 (2017) 117–127, https://doi.org/10.1002/cpch.20.
[49] M.E. Matlashov, V.V. Belousov, G. Enikolopov, How much H(2)O(2) is produced by recombinant D-amino acid oxidase in mammalian cells? Antioxid. Redox Signal. 20 (2014) 1039–1044, https://doi.org/10.1089/ars.2013.5618.
[50] E.S. Arner, A. Holmgren, The thioredoxin system in cancer, Semin. Cancer Biol. 16 (2006) 420–426, https://doi.org/10.1016/j.semcancer.2006.10.009.
[51] T.C. Karlenius, K.F. Tonissen, thioredoxin and cancer: a role for thioredoxin in all States of tumor oxygenation, Cancers 2 (2010) 209–232, https://doi.org/10.3390/cancers2020209.
[52] J. Zhang, X. Li, X. Han, R. Liu, J. Fang, Targeting the thioredoxin system for cancer therapy, Trends Pharmacol. Sci. 38 (2017) 794–808, https://doi.org/10.1016/j.tips.2017.06.001.
[53] O. Rackham, A.M. Shearwood, R. Thyer, E. McNamara, S.M. Davies, B.A. Callus, A. Miranda-Vizuete, S.J. Berners-Price, Q. Cheng, E.S. Arner, A. Filipovska, Substrate and inhibitor specificities differ between human cytosolic and mitochondrial thioredoxin reductases: implications for development of specific inhibitors, Free Radic. Biol. Med. 50 (2011) 689–699, https://doi.org/10.1016/j.freeradbiomed.2010.12.015.
[54] A. Degrossoli, A. Muller, K. Xie, J.F. Schneider, V. Bader, K.F. Winklhofer, Neutrophil-generated HOCl leads to non-specific thiol oxidation in phagocytized bacteria, vol. 7, 2018, published online EpubMar 6 ⟨http://dx.doi.org/10.7554/eLife.32288⟩.
[55] A. Muller, J.F. Schneider, A. Degrossoli, N. Lupilova, T.P. Dick, L.I. Leichert, Systematic in vitro assessment of responses of roGFP2-based probes to physiologically relevant oxidant species, Free Radic. Biol. Med. 106 (2017) 329–338, https://doi.org/10.1016/j.freeradbiomed.2017.02.044.
[56] J. Birk, M. Meyer, I. Aller, H.G. Hansen, A. Odermatt, T.P. Dick, A.J. Meyer, C. Appenzeller-Herzog, Endoplasmic reticulum: reduced and oxidized glutathione revisited, J. Cell Sci. 126 (2013) 1604–1617, https://doi.org/10.1242/jcs.117218.